Plasma Sources Science and Technology

PAPER

Time-resolved characterization of a free plasma jet formed off the surface of a piezoelectric crystal

To cite this article: Jinyu Yang *et al* 2020 *Plasma Sources Sci. Technol.* **29** 045016

IOP Publishing Plasma Sources Science and Technology
Plasma Sources Sci. Technol. 29 (2020) 045016 (10pp) https://doi.org/10.1088/1361-6595/ab7987

Time-resolved characterization of a free plasma jet formed off the surface of a piezoelectric crystal

Jinyu Yang[1], **Seong-Kyun Im**[1,2,4] and **David B Go**[1,3,4]

[1] Department of Aerospace and Mechanical Engineering, University of Notre Dame, Notre Dame, IN 46556 United States of America
[2] School of Mechanical Engineering, Korea University, Republic of Korea
[3] Department of Chemical and Biomolecular Engineering, University of Notre Dame, Notre Dame, IN 46556 United States of America

E-mail: sim3@korea.ac.kr and dgo@nd.edu

Received 10 December 2019, revised 6 February 2020
Accepted for publication 24 February 2020
Published 3 April 2020

Abstract

When a piezoelectric transformer (PT) is actuated by a low input voltage (~10 V), electromechanical coupling leads to a very high (~10^3 V) surface potential at the distal end that can ionize the surrounding gas and lead to a plasma jet emanating from the surface. PTs are attractive for non-equilibrium plasma generation because of their simple operation, low required input voltage, and low power consumption. In this work, the time-resolved characteristics of the free surface plasma jet generated by a PT operating in open air have been investigated. The temporal evolution of the PT-driven plasma was visualized by using an intensified CCD camera and plasma formation was correlated with the current behavior of the plasma jet. Notably, the plasma formation is a discrete process, appearing at a relatively fixed phase of the sinusoidal input, and the strongest plasma jet appears at the end of the positive half-cycle. Simultaneous measurements of the current show that the discharge current response is consistent with the chaotic mode for a plasma jet and appears statistically about a 1 μs earlier than plasma jet light emission, which indicates that there is a strong afterglow. With a low input voltage required for operation, these types of PT-driven plasma jets could have wide utility in emerging plasma applications beyond the laboratory, such as in healthcare and water treatment.

Keywords: piezoelectric transformer, free plasma jet, streamer corona, plasma afterglow

1. Introduction

Atmospheric pressure gas discharges have been extensively utilized in a variety of fields owing to their unique physical and chemical properties [1]. One of the most promising plasma devices is the non-equilibrium plasma jet (or cold plasma jet) because it extends the discharge region outside of the gap of electrodes and allows interaction with remote subjects [2]. Common approaches to generating a plasma jet require high-voltage power sources with frequencies spanning pulsed DC (kHz) to microwaves (GHz) [3–10]. Pulsed or high-frequency operation temporally limits the applied field, which prevents the transition from non-equilibrium conditions to equilibrium conditions. However, the reliance on high-voltage, high-frequency power supplies constrains most of these devices to laboratory settings, limiting their application as portable devices in non-laboratory, field applications. Since these devices can be used for applications including water purification [11, 12], wound healing [13–15], and even agricultural fertilization [16, 17], technologies that enable portable plasma sources could be profoundly impactful.

To date, there have been a variety of battery-powered devices that have been demonstrated to meet this field-portability challenge [18, 19]. However, the electrical circuitry for these systems are generally complex and require batteries that

[4] Authors to whom any correspondence should be addressed.

ultimately need to be recharged or replaced. An alternative approach would rely on an energy conversion strategy where either mechanical energy [20] or thermal energy [21] is directly converted into plasma generation, foregoing the need for any electrical power supply at all. To that end, the piezoelectric effect of non-centrosymmetric crystals, such as lead zirconate titanate ($Pb[Zr_{(x)}Ti_{(1-x)}]O_3$, PZT) and lithium niobate ($LiNbO_3$, LN), offer one potential approach to overcoming the need for a high-voltage power supply.

Non-centrosymmetric crystals are materials whose crystal lattice lacks an inversion center, which in turn allows them to be easily polarized. One subset of these are piezoelectric crystals, where mechanical stress can induce strong polarization and in turn lead to high electric potentials on the crystal surface (called the direct piezoelectric effect). If the mechanical stress is applied properly (e.g. periodic with sufficiently high magnitude and/or frequency), the induced surface potential can breakdown the surrounding gas and produce a non-equilibrium gas discharge. To our knowledge, while such piezoelectric materials can be used for spark generation (such as in spark igniters), there is no published report on using the direct piezoelectric effect for non-equilibrium plasma generation. One of the limiting factors is the lack of comprehensive knowledge about the fundamental mechanisms for mechanical-to-plasma generation and the difficulty of providing a proper mechanical stress. To that end, piezoelectrics materials are most often utilized for plasma generation in the form of piezoelectric transformers (PTs).

PTs are compact, lightweight, and high-efficiency electrical transformers that can produce high-voltage AC output in response to periodic mechanical stress induced by a low-voltage AC input [22]. They have been widely used as high-voltage sources in cold cathode fluorescent lamps (CCFLs) to backlight liquid crystal displays (LCDs) [22, 23] and as AC-DC converters [24]. First demonstrated as a plasma source by Itoh *et al* [25], PTs have now been incorporated into dielectric barrier discharges (DBDs), corona discharges, and glow discharges [26–33]. They have also been used to produce plasma jets, with a number of groups using cylindrical-tube shaped PTs [34–36]. More recently, Johnson *et al* [37] characterized the electrical and optical properties of helium and argon plasma jets driven by a versatile rectangular PT and compared it against a high-voltage driven counterpart. Similarly, Babij *et al* [38] designed and tested a PT-powered capillary plasma jet system serving as an ionization source for ambient mass and ion mobility spectrometry. In these studies, as well as some on corona discharges driven by PTs [28], the plasma initiated from the end of a sharp-tipped electrode attached to the high-voltage output surface of the PT. However, utilizing attached electrodes may not be the most efficient approach because high surface potentials on the edges of the PT itself can also ionize the surrounding gas and lead to the loss of energy [39].

An alternative approach is to use PT itself as one of the electrodes, where the plasma forms directly off the high-voltage surface of the PT. In our prior work, we showed that a plasma streamer can be formed directly from the corners of a rectangular PT crystal without any second grounded electrode [39]. When operating at a sufficiently high input voltages ($\geqslant$20 V_{rms}), this streamer shares many characteristics with a plasma jet, with the exception that it is formed off a free surface as opposed to the conventional picture of being formed in a constrained gas flow [40]. These free plasma jets open the possibility of using PTs to efficiently produce plasma jets without a high-voltage power supply or a source of forced gas flow.

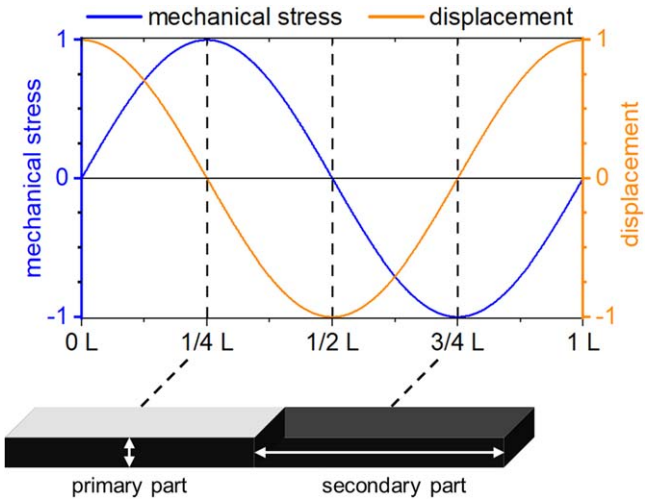

Figure 1. Schematic of a Rosen-type PZT PT utilized for this work. The gray areas on the top and bottom (hidden) of the primary part represent the input electrodes. White arrows indicate the polarization directions of each part. The orange and blue lines in the plot represent the displacement wave and mechanical stress formed when running the PT at its second harmonic, respectively.

Vital to the development of an energy conversion plasma source that utilizes the piezoelectric effect is establishing a better understanding about how the plasma forms on the piezoelectric surface. In this paper, we report time-resolved measurements of a free plasma jet formed off the surface of a commercial PT actuated by a low-voltage (~25 V_{rms}) AC input. High-speed imaging reveals the temporal evolution of the discharge from the surface and simultaneous high-speed electrical measurements show the relationship between the current and plasma emission. We found that the plasma itself forms consistently at a certain phase in the low-voltage actuation cycle, sometimes forming a single jet and sometimes forming a second jet, and statistical analysis reveals that the plasma jet is operating in a chaotic mode. A comparison of the emission and electrical characteristics show that the plasma emission is phase-shifted from the peak current, typical of an afterglow.

2. Experimental method

2.1. Piezoelectric transformer

The piezoelectric crystal employed in this paper is a Rosen-type PT [41], shown in figure 1. It is a combination of two PZT crystals whose polarizations are perpendicular to each

other. Analogous to the electromagnetic coupling in a conventional magnetic core transformer, a PT converts low-voltage AC input to a high-voltage AC output through innate electromechanical coupling: the input signal V_{in} induces the converse piezoelectric effect in the primary part of the PT, leading to a standing displacement wave in the PZT crystal that subsequently applies mechanical stress to the adjacent orthogonally-polarized PZT crystal (secondary part), which in turn forms an output V_{out} due to the direct piezoelectric effect. The voltage gain of a Rosen-type PT can be evaluated by

$$\frac{V_{out}}{V_{in}} \propto k_t k_l Q \frac{L}{H}, \tag{1}$$

where k_t are k_l are transverse and longitudinal piezoelectric coupling coefficients, respectively [42], Q is the mechanical quality factor, L is the total length of the PT, and H is the thickness of the crystal. The energy conversion changes in response to the frequency of the AC input, and the most efficient conversion occurs at harmonics of the resonant frequency of the crystal, with voltage gains on the order of 10^2–10^3 possible [37, 39, 43]. Practically, the PT is mounted such that it is pinned at the nodes of the induced standing wave. An input AC voltage is applied to the faces of the primary part of the PT, and the distal end of the secondary part achieves the highest surface potential and voltage output.

In this work, we used a 53 mm long × 7.5 mm wide × 2.6 mm thick commercially-available PZT PT (Steiner & Martins, INC model SMSTF68P10S9). The PT was operated in its second harmonic mode (second resonant frequency) such that the PT was mounted on an apparatus that pinned the PT at the nodes of the displacement wave, as shown in figure 1 (along with the induced mechanical stress). Nodes are located at $L/4$ and $3L/4$, indicated by the black dashed lines in figure 1. Plastic, rather than metal, mounts were employed to avoid triple-point enhancement, which can cause gas breakdown at the node at $3L/4$ [44]. The as-purchased PT is designed to be a high-voltage power source, such that it comes with a silver electrode on the surface of the secondary electrode. In order to better understand the discharge produced purely on the PZT surface and not influenced by the material coated on the surface [44], the native silver output electrode was etched away using nitric acid before conducting this work. Three different PTs were utilized to confirm that the observed behavior was repeatable; all three produced similar results, and the data presented here is for only one of those PTs.

2.2. Experimental approach

In order to operate the PZT PT at its second resonant frequency, the input current and voltage were simultaneously monitored. As the frequency is varied and the PT approaches resonance (67.6 kHz for the PT used here), the input current becomes in phase with the input voltage, and its magnitude increases significantly due to a decrease in the PT's impedance. Figure 2 shows the schematic of the experimental apparatus for this study. The input voltage was generated by amplifying a sinusoidal waveform from a function generator

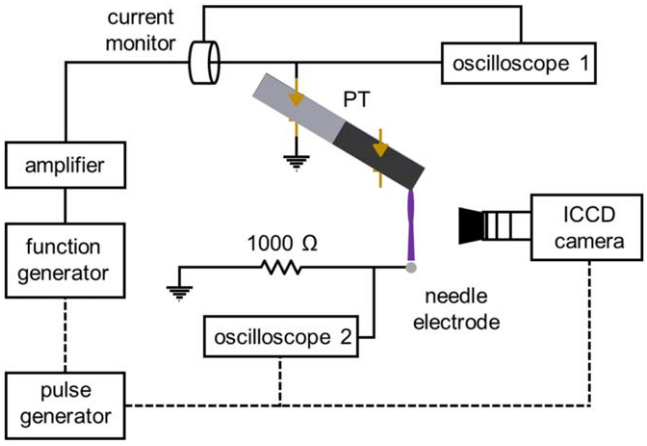

Figure 2. Schematic of the experimental apparatus employed to form a free plasma jet (the violet region) off the surface of a PT. The dashed lines represent cables to trigger the oscilloscope and ICCD camera. The golden arrows represent plastic components used to mount the PT at the nodes of the second harmonic displacement wave.

(Keysight 33210A) through an RF amplifier (Powertron, Model 509A) and measured using a high-frequency voltage probe (Tektronix TPP0101). Input current was measured with a Pearson current monitor (Model 4100). Both voltage and current measurements were monitored using a digital oscilloscope (GW Instek GDS-1054B) at the sampling rate of 200M samples per second.

Time-resolved images of the free plasma jet were taken with an ICCD camera (Andor iStar intensified sCMOS) equipped with a 60 mm lens (Nikon AF Micro Nikkor, 60 mm, 1:2.8 D) and a series of four extension tubes with a total length of 95.5 mm. Since the free plasma jets originate at the corners of the PT and propagate through free space with various azimuthal angles and polar angles, a larger depth of field (DOF) was required. To compensate the smaller DOF of the imaging system, the PT was placed at an angle to the centerline of the camera such that the camera was orthogonal to the plasma jet as shown in figure 2.

Simultaneously, the discharge current of the plasma jet was also measured at an auxiliary needle electrode downstream from the PT's corner. The electrode was connected to a 1000 Ω resistor, and the current was recorded with a second digital oscilloscope (Tektronix DPO3012) at a sampling rate of 250 M samples per second. In most conventional capillary plasma jet configurations or those formed by an electrode attached to a PT, a flat plate electrode is used to measure the discharge current [37, 45]. The criterion for auxiliary electrode selection for this work was to form a discharge that was as visually similar to a discharge without an electrode to reflect the behavior of a freely propagating jet. During a series of preliminary experiments, we found that the shape and size of the auxiliary electrode, unsurprisingly, affected the size and shape of the free plasma jet and its discharge current. Specifically, larger area electrodes such as flat plates cause the plasma jet to spread radially. Additionally, when the electrode is placed too close to the PT corner (<10 mm), the plasma jet can be significantly enhanced and even form continuous

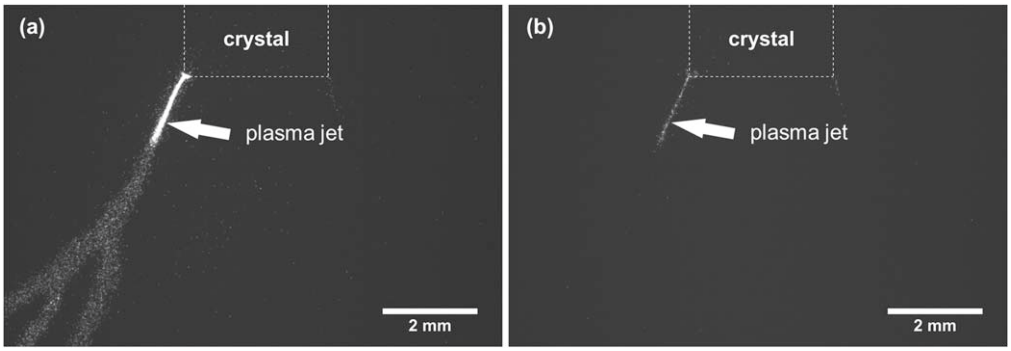

Figure 3. Images taken at the same phase but different cycles of the input voltage. The plasma jet in panel (a) has a higher intensity (brighter) and stretches a longer distance from the PT. In contrast, the plasma jet in panel (b) is weaker and shorter. Both images were taken at a delay of 7.0 μs during the period of the input voltage.

sparks. Through trial and error, it was determined that a needle placed 15 mm downstream from the PT's corner had a small effect on the free plasma jet and therefore, was used here for current measurements.

2.3. Phase-locked optical and electrical measurements

The major contribution of this study is the visualization of the temporal evolution of the free plasma jet propagating from the PT surface. To map the time evolution, one period of the input voltage ($\sim$14.8 μs) was separated into multiple phases, each with a time interval of 250 ns, and the ICCD camera was synchronized to capture the discharge phenomenon for each phase. In general, there is some stochastic behavior in the formation of the plasma jet, and the overall light emission for a single occurrence is variable and low, as illustrated in figure 3. Therefore, in this work, we present the integrated emission (light intensity) across 1000 sequential ICCD images over 1000 cycles of operation. Although these images do not capture cycle-to-cycle variation, they do reflect the average periodic behavior of plasma jet formation. Because of the low frame rate of the ICCD camera, the PT must be run for more than 1 min to obtain 1000 images. However, long runtimes can overheat the PT, causing a shift in the resonant frequency [46, 47]. Instead of operating the PT in a continuous mode, a burst mode with a period of 100 ms and a duty cycle of 14.8% (14.8 ms) was utilized. During the burst period, images were acquired at the 501st input voltage cycle, and images from 1000 successive burst periods were recorded. Using the 501st cycle assumes that the discharge formation becomes quite stable after 500 cycles within a single burst period and thus accurately reflects operation in a continuous mode. The selection of the 501st cycle was achieved by setting a proper delay time ($\sim$7.4 ms) on the pulse generator (Quantum 9520 Series). The intrinsic delays of the pulse generator and ICCD camera have been taken into account while selecting the imaging cycle. The background was subtracted from the integrated images by using an image processing software (ImageJ) [48]. The secondary oscilloscope (Tektronix DPO3012) was also triggered by the pulse generator and simultaneously recorded the discharge current of the 501st input voltage cycle.

3. Results

3.1. PT-driven free plasma jet

Figure 4 shows a time-integrated image of a plasma jet formed off the left corner of a PT, acquired over 5000 input voltage cycles (0.5 s exposure time) and taken with a Canon EOS Rebel T3i camera. Qualitatively the plasma plume shares many characteristics with conventional plasma jets formed by gas flows through capillaries [40] in that it propagates into free space with a well-defined shape, although its tail is more diffuse than conventional plasma jets. The visible length of the plasma plume without an auxiliary electrode is approximately 15–20 mm when observed by the naked eye, which is similar to the plasma jet length reported in [37].

A plasma jet is generally defined as plasma streamers (or ionization waves) guided by a flowing gas channel into a surrounding different ambient gas (e.g. Ar into N_2 or He into air) [2, 49]. The different gases are important because the guiding gas is easier to ionize and thus confines the plasma streamers to the guiding gas jet plume [50]. In contrast, here the plasma streamers are forming off the surface of the PT into free (unbounded) space; there is no low-ionization-energy guiding flow. In fact, a more precise name, and perhaps better analog, would be a corona streamer [51]. However, as opposed to corona streamers that typically branch and propagate stochastically, we found that the PT plasma streamers occurred in a repeatable and reproducible manner over thousands of pulsed cycles and shared common electrical features with conventional plasma jets, as will be shown in the following sections. Due to these common features and the free propagating nature, the discharge analyzed in this work is referred to as a free plasma jet.

3.2. Time-resolved measurements

Figure 5(a) shows the normalized input voltage throughout one period. The period begins at a delay time of 0 μs and is defined as the time during the input voltage when the voltage is 0 V. The black regions plotted on top of the input voltage curve each have a duration of 250 ns and reflect periods where the plasma jet was interrogated using phase-locked imaging and current measurements.

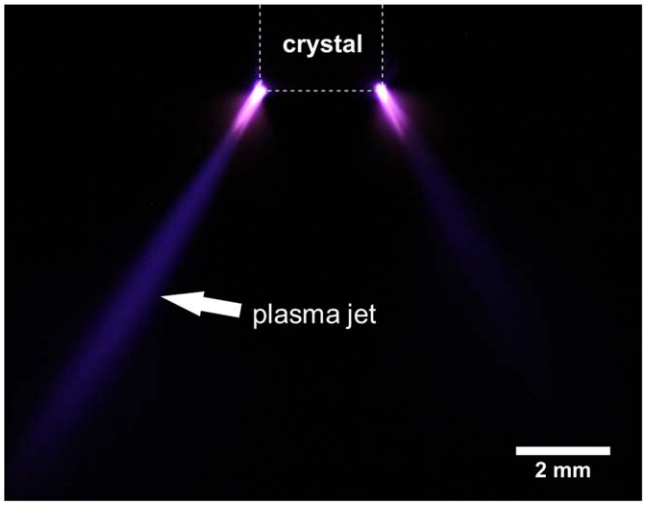

Figure 4. Time-integrated image over 5000 input voltage cycles (0.5 s camera exposure time) of a plasma jet formed from the corner of a PT crystal. The boundary of the crystal is outlined with the white dashed line. The PT was actuated by a sinusoidal input voltage of 25 V_{rms} in its second harmonic mode at a frequency of 67.6 kHz.

The plasma jet current was measured at the auxiliary electrode [52], and figures 5(b) and (c) show two measurements of discharge current produced while operating the PT. The displacement current of the PT itself has been subtracted by fitting the raw current data with an asymmetric least-square smoothing algorithm [53]. Generally, as illustrated in figure 5(b), a distinct, single strike was observed during the positive half-cycle of the input voltage. However, double strikes were also measured as shown in figure 5(c). Similar behavior was also observed for the negative half-cycle, but the current magnitudes of the spikes were about an order of magnitude smaller than for the positive half-cycle.

The phenomenon of the secondary strike is analogous to a backward ionization wave that has been observed in conventional plasma jets and is often called a restrike. However, in this work, the average time lag between the first and the second strikes is 597 $\pm$ 292 ns, which is much longer than the typical time lag for a restrike, which is on the order of 10 ns [54]. Generally, the propagation of a restrike relies on the residual charges in the ionization channel [52], which have a very short lifetime ($\sim$100 ns) for discharges operating at atmospheric pressure [55]. The time delay between two strikes measured here is much longer than the lifetime of residual charges, suggesting that there is likely little to no remaining charge in the ionization channel to initiate a restrike. We believe that the secondary strike is a second streamer that is independent of the first one, and the double strike phenomenon is similar to the multiple micro discharges formed in a DBD or a corona discharge [39]. However, the fact that only single or double strikes are ever observed (as opposed to triple or quadruple) and that they occur at consistent phases in the period reflects how this PT-driven free plasma jet is distinct from typical stochastic DBD or corona discharge behavior.

Figure 6 shows integrated images (over 1000 cycles) taken at different phases within one input voltage period; the

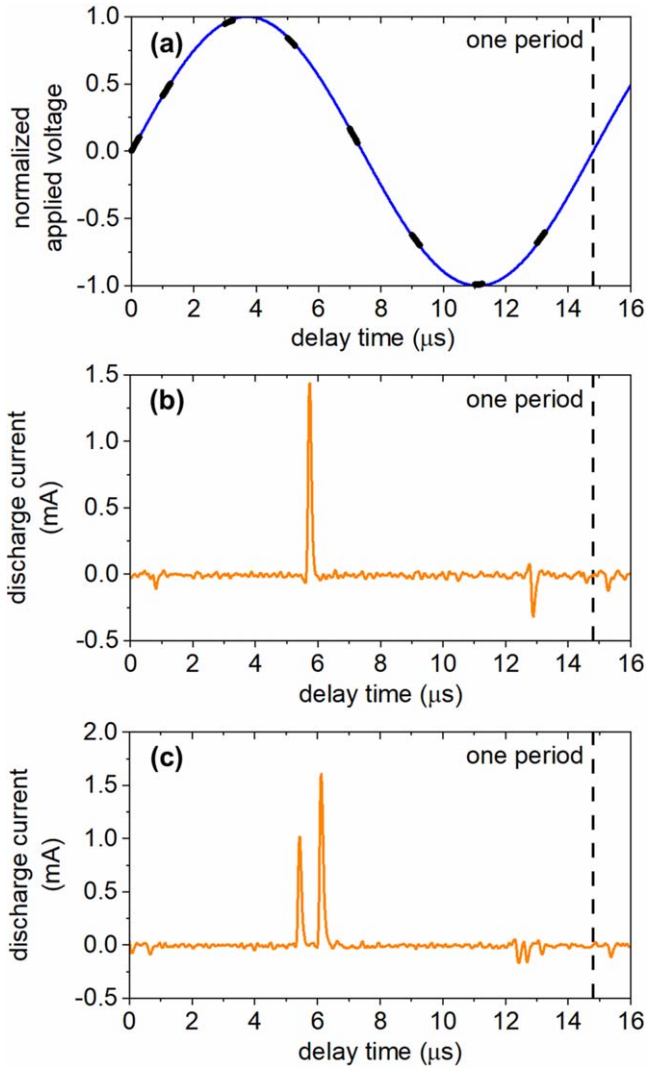

Figure 5. (a) Normalized input voltage throughout an actuation cycle. The black regions are 250 ns phases where phase-locked ICCD imaging and current measurements were acquired. Representative measured current as a function of the delay time for a case where there is (b) a single strike and (c) double strikes. The PT was actuated by a sinusoidal input voltage of 25 V_{rms} in its second harmonic mode at a frequency of 67.6 kHz.

boundary of the PT is outlined by the white dashed lines. The camera exposure during each phase (250 ns) is too long to track the motion of the extremely fast streamer header ($\sim 10^4$–10^5 m s^{-1}) [5, 56], but is sufficiently fast to show the discharge evolution as a function of time. Interestingly, at the beginning of the input voltage cycle, when the delay time is 0 μs and the input voltage is 0 V, a faint plasma from the preceding cycle is still visible. This can be attributed to the phase difference between the PT's input and output. The electromechanical coupling in the PT results in a time lag between the input voltage and the induced polarization at the distal end, causing the output voltage to be phase shifted. Ideally, the output voltage would be measured directly, but utilizing a contact voltage probe would necessarily interfere with plasma generation. Teranishi *et al* developed contactless methods to take output voltage data for PT systems with

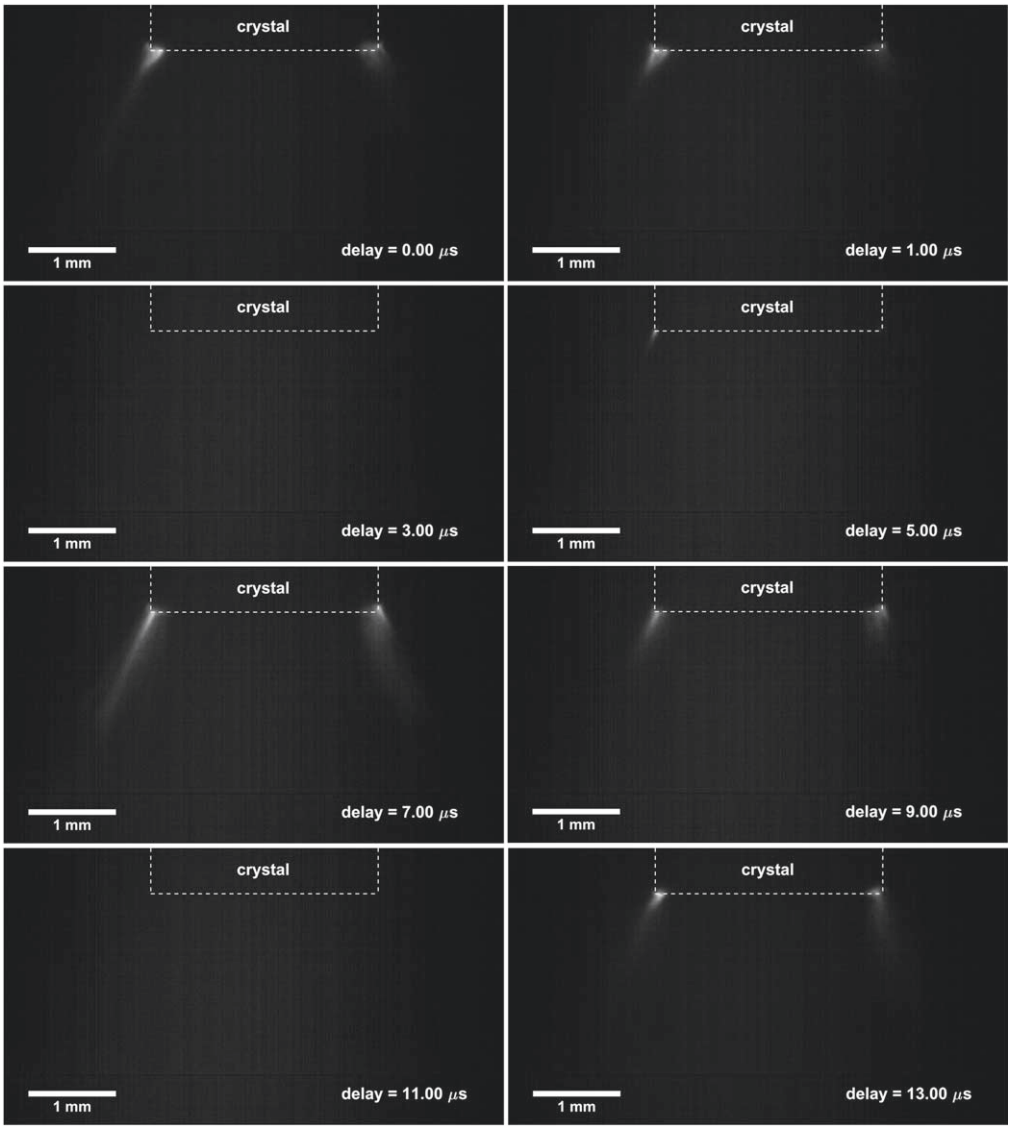

Figure 6. Time-integrated images taken at different phases of an input voltage period. The white dashed line represents the outline of the PT. The delay time with respect to 0 μs is identified at the bottom right of each image. The PT was actuated by a sinusoidal input voltage of 25 V_{rms} in its second harmonic mode at a frequency of 67.6 kHz.

resistance loads [57, 58]. However, those methods are not suitable for the PT running as a plasma source because the output behaves distinctly for different loads that it is driving [47]. Here, if we assume the phase shift of the output voltage is approximately $\pi/2$ as reported in [37] and approximate the voltage gain of the PT to be 10^3, the output voltage at 0 μs in the input voltage cycle thus corresponds to negative output voltage on the order of -10^3 V, which would be enough to breakdown the air. After 1 μs delay, the plasma emission begins to fade, and finally no light is observed at 3 μs as the plasma jet initiated in the previous cycle terminates. The ignition of a new plasma jet and initial observation of emission light appears at 5 μs and starts to become stronger as the cycle progresses. The most intense light emission among the images shown in figure 6 appears at 7 μs, at which a jet plume is formed off the left corner of the PT. From 7 μs to 9 μs, the emission light begins to fade again and the jet becomes noticeably shorter. No emission light is observed after 11 μs until 13 μs, when a plasma jet ignited by the negative voltage cycle initiates. This negative cycle plasma jet continues through the end of the cycle and into the next period, corresponding to the initial image at 0 μs as discussed above.

Figure 7 quantitatively shows the evolution of the normalized plasma emission intensity as a function of the time delay throughout a single cycle along with the normalized input voltage. In this case, the emission intensity is defined as the sum of the image intensity for all pixels within the plasma jet plume off the left corner of the crystal. The intensity is then normalized by the maximum intensity in the cycle, which occurs at a time delay of 6.5 μs. The trend shown in this figure is in good agreement with the observations shown in figure 6. During the portion of the half-cycle where the input voltage is falling (5–10 μs), the output surface potential is increasing due to the time lag between input and polarization, as discussed earlier; the PT works as an anode and produces cathode-directed streamers (positive streamers).

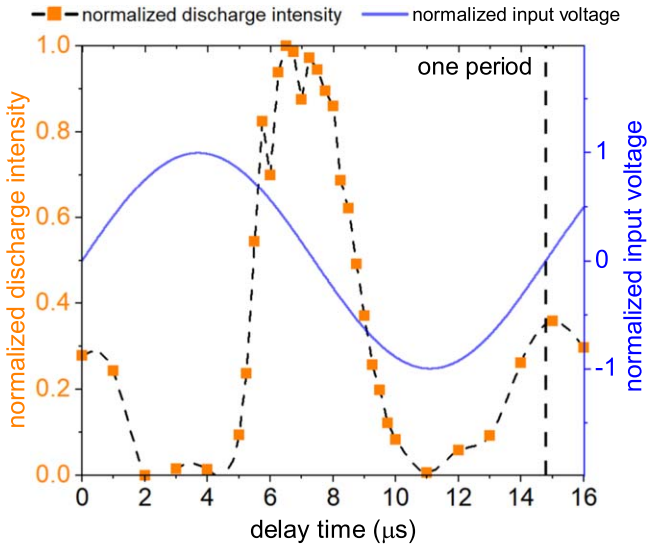

Figure 7. Plasma emission intensity changes as a function of the delay time, where the black dashed line illustrates the trend. Intensities were normalized by the strongest emission during the cycle, which occurred at 6.5 μs. Normalized input voltage (solid blue line) is included as a reference. The PT was actuated by a sinusoidal input voltage of 25 V_{rms} in its second harmonic mode at a frequency of 67.6 kHz.

Anode-directed negative streamers appear shortly after 12 μs and continue into the following cycle due to the phase lag. Clearly, emission light intensities for negative streamers are much lower than positive streamers. Additionally, no plasma emission was observed between the half-cycles, for example at the delay times of 3 and 11 μs, respectively.

Measurements of discharge current show a discrepancy in magnitude between the positive and negative half-cycles, as shown in figures 5(b) and (c). Large positive currents appear when the PT is producing positive streamers, whereas the negative currents are one order of magnitude smaller than their positive counterparts. This is consistent with the emission intensities shown in figure 7 as well as the shorter extent of the plasma jets shown in figure 6. Notably, similar phenomena have been also reported in [37, 45, 59, 60] for conventional plasma jets. Previous studies have shown that higher voltages are required to initialize a negative streamer than a positive streamer [61, 62]. This is because the header of a negative streamer consists of electrons that are more diffusive than the ions in a positive streamer header such that greater external energy (applied voltage) is required to sustain directed charge transport. In the case of these PT measurements, it is likely that the output surface voltage produced by our PT was not high enough to produce strong negative streamers.

3.3. Statistical characterization

Statistical analysis of over 1000 positive discharge currents was conducted and compared to the emission response of the plasma jets. The majority of plasma jets are formed as single strikes (74.9%) while the remaining were double strikes (25.1%). Interestingly, positive current strikes (or the first strike if there are two) appear at a mean delay time of 5.65 $\pm$ 0.36 μs (at one standard deviation) with a mean magnitude of 2.03 mA that varies as much as 63.4%. This relatively large variation in the phase response of the positive strike indicates that the free plasma jets were running in what has been termed a 'chaotic mode' [45], although the plots in figures 5(b) and (c) appear more like a bullet mode. The average duration of positive current spikes, defined by the width of the current spike, is 0.42 $\pm$ 0.06 μs which is on the same order of magnitude as the lifetime of a conventional plasma jet driven by a PT [37].

Figure 8(a) shows a stacked histogram plot of the phase response of these positive strikes along with the phase response of the plasma emission from figure 7. We observe that the majority of positive strikes are distributed between delay times of 4.5–7.5 μs, and take Gaussian distributions, consistent with stochastic (chaotic) formation. In contrast, strong plasma emission appears between delay times of 6.5–8.0 μs. In addition, no positive strike current has been measured beyond 8 μs, whereas measurable plasma emission occurs well after that, as shown in figure 8(b) where the light was measured at a delay of 9.5 μs. This shift in phase indicates that the free plasma jet produces a strong afterglow, which appears to be the source of the light emission captured after 8 μs. One common method for proving the presence of afterglow is to conduct time-resolved spectroscopy of metastable species; this could be an interesting direction for our future work on these PT-driven free plasma jets.

While the appearance of the afterglow was readily apparent for the positive half-cycle, it was difficult to extract negative current spikes from raw current measurements due to their relatively smaller magnitudes compared to the displacement current and signal noise (see figures 5(b) and (c)). As such, we could not create a meaningful distribution of negative current spikes that could be compared with the plasma emission intensity to reveal whether there is also a time lag and possible afterglow during the negative half-cycle.

4. Conclusions

Piezoelectric crystals have the potential to be the foundation for energy conversion plasma sources that convert mechanical energy directly into atmospheric-pressure plasmas. In this work, a PT has been utilized as a model system to study the formation of free plasma jets directly off the surface of the piezoelectric crystal, and PTs themselves are attractive candidates for plasma sources as they are compact and lightweight, operate with high efficiency, and are capable of generating large voltage gains. In this study, we formed a gas discharge off the surface of a commercial PZT PT. The discharge shares many qualities with conventional plasma jets but is not constrained by a low-ionization energy guiding flow, such that it is referred to as a free plasma jet. Time-resolved and simultaneous imaging and current measurements show that the plasma jet formation is a discrete process, where

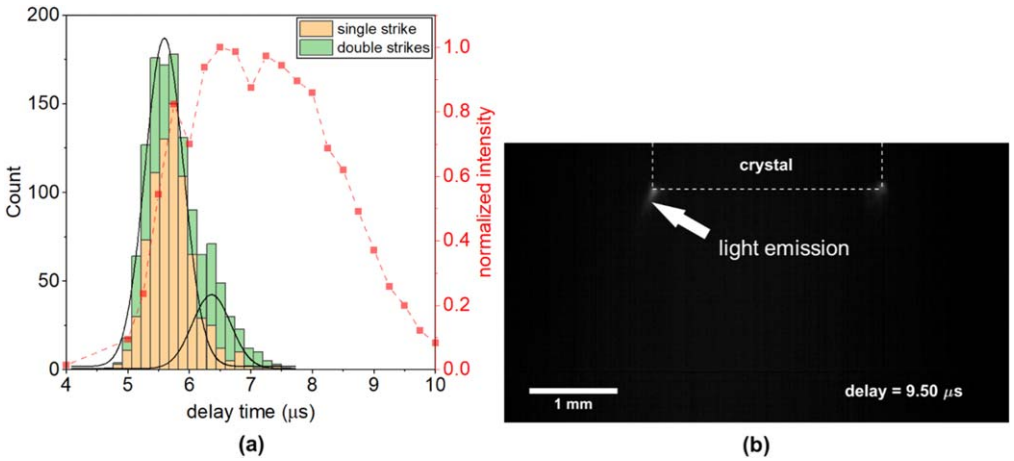

Figure 8. (a) Stacked histogram plot shows the distribution of time delays of measured positive current spikes for single and double strikes, respectively. The plasma emission intensity (red symbols with red dashed line) shows that there is a phase lag between the current spike and light emission, indicative of an afterglow. Black lines are the Gaussian fits of current spikes for single strikes and the first strike of double strikes (taller), and for the second strike of double strikes (shorter). Panel (b) shows an integrated image taken at the delay time of 9.5 μs at which no discharge current has been measured, but a small bright region can be found around the corners of the PT, which indicates that light emission had been produced during camera exposure.

long, high-intensity plasma jets only appear during the falling portion of the positive half-cycle of the input, and weaker, shorter plasma jets form in the rising portion of the negative half-cycle. Statistical analysis of the current and light emission for the positive current strikes indicates that the plasma jet operates in a chaotic mode and produces an afterglow. Further time-resolved studies on the formation of the plasma jet, including the surface electric field on the piezoelectric, and its relevant plasma properties will help develop a comprehensive understanding of PTs and PT-driven plasma jets, laying the foundation for their use in applications outside the laboratory.

Acknowledgments

This work is based on support from the National Science Foundation under Award No. PHY-1804091.

ORCID iDs

Jinyu Yang https://orcid.org/0000-0003-4304-2289
Seong-Kyun Im https://orcid.org/0000-0002-7449-4336
David B Go https://orcid.org/0000-0001-8948-1442

References

[1] Adamovich I *et al* 2017 The 2017 plasma roadmap: low temperature plasma science and technology *J. Phys. Appl. Phys.* **50** 323001
[2] Lu X, Laroussi M and Puech V 2012 On atmospheric-pressure non-equilibrium plasma jets and plasma bullets *Plasma Sources Sci. Technol.* **21** 034005
[3] Förster S, Mohr C and Viöl W 2005 Investigations of an atmospheric pressure plasma jet by optical emission spectroscopy *Surf. Coat. Technol.* **200** 827–30
[4] Zhang J, Sun J, Wang D and Wang X 2006 A novel cold plasma jet generated by atmospheric dielectric barrier capillary discharge *Thin Solid Films* **506–507** 404–8
[5] Teschke M, Kedzierski J, Finantu-Dinu E G, Korzec D and Engemann J 2005 High-speed photographs of a dielectric barrier atmospheric pressure plasma jet *IEEE Trans. Plasma Sci.* **33** 310–1
[6] Kim D B, Rhee J K, Moon S Y and Choe W 2006 Study of geometrical and operational parameters controlling the low frequency microjet atmospheric pressure plasma characteristics *Appl. Phys. Lett.* **89** 061502
[7] Janča J, Klı M, Slavı P and Zajı L 1999 HF plasma pencil—new source for plasma surface processing *Surf. Coat. Technol.* **116–119** 547–51
[8] Stoffels E, Flikweert A J, Stoffels W W and Kroesen G M W 2002 Plasma needle: a non-destructive atmospheric plasma source for fine surface treatment of (bio)materials *Plasma Sources Sci. Technol.* **11** 383–8
[9] Stonies R, Schermer S, Voges E and Broekaert J A C 2004 A new small microwave plasma torch *Plasma Sources Sci. Technol.* **13** 604
[10] Shimizu T *et al* 2008 Characterization of microwave plasma torch for decontamination *Plasma Process. Polym.* **5** 577–82
[11] Foster J, Sommers B S, Gucker S N, Blankson I M and Adamovsky G 2012 Perspectives on the interaction of plasmas with liquid water for water purification *IEEE Trans. Plasma Sci.* **40** 1311–23
[12] Foster J E 2017 Plasma-based water purification: challenges and prospects for the future *Phys. Plasmas* **24** 055501
[13] Weltmann K D, Kindel E, Brandenburg R, Meyer C, Bussiahn R, Wilke C and Woedtke T V 2009 Atmospheric pressure plasma jet for medical therapy: plasma parameters and risk estimation *Contrib. Plasma Phys.* **49** 631–40
[14] Kong M G, Kroesen G, Morfill G, Nosenko T, Shimizu T, Dijk J V and Zimmermann J L 2009 Plasma medicine: an introductory review *New J. Phys.* **11** 115012
[15] Haertel B, von Woedtke T, Weltmann K-D and Lindequist U 2014 Non-thermal atmospheric-pressure plasma possible application in wound healing *Biomol. Ther.* **22** 477–90

[16] Thirumdas R, Kothakota A, Annapure U, Siliveru K, Blundell R, Gatt R and Valdramidis V P 2018 Plasma activated water (PAW): chemistry, physico-chemical properties, applications in food and agriculture *Trends Food Sci. Technol.* **77** 21–31

[17] Ito M, Oh J S, Ohta T, Shiratani M and Hori M 2018 Current status and future prospects of agricultural applications using atmospheric-pressure plasma technologies *Plasma Process. Polym.* **15** 1700073

[18] Pei X, Lu X, Liu J, Liu D, Yang Y, Ostrikov K, Chu P K and Pan Y 2012 Inactivation of a 25.5 μm *Enterococcus faecalisbiofilm* by a room-temperature, battery-operated, handheld air plasma jet *J. Phys. Appl. Phys.* **45** 165205

[19] Parkey J, Cross J, Hayes R, Parham C, Staack D and Sharma A C 2015 A battery powered, portable, and self-contained non-thermal helium plasma jet device for point-of-injury burn wound treatment *Plasma Process. Polym.* **12** 1244–55

[20] Tang X and Staack D 2019 Bioinspired mechanical device generates plasma in water via cavitation *Sci. Adv.* **5** eaau7765

[21] Johnson M J, Linczer J and Go D B 2014 Thermally induced atmospheric pressure gas discharges using pyroelectric crystals *Plasma Sources Sci. Technol.* **23** 065018

[22] Vazquez Carazo A 2016 Piezoelectric transformers: an historical review *Actuators* **5** 12

[23] Ben-Yaakov S and Peretz M M 2007 Cold cathode fluorescent lamps driven by piezoelectric transformers: stability conditions and thermal effect *IEEE Trans. Power Electron.* **22** 761–8

[24] Park Y W 2010 Electrical properties of a piezoelectric transformer for an AC-DC converter *J. Korean Phys. Soc.* **57** 1131–3

[25] Itoh H, Suzuki T and Suzuki S 2000 Observation of a Silent Discharge using a Piezoelectric Transformer in Oxygen *American Physical Society 53rd Annual Gaseous Electronics Conf. (Houston, TX)* JWP.081

[26] Itoh H, Teranishi K and Suzuki S 2002 Observation of light emissions around a piezoelectric transformer in various gases *IEEE Trans. Plasma Sci.* **30** 124–5

[27] Teranishi K, Itoh H and Suzuki S 2002 Dynamic behavior of light emissions generated by piezoelectric transformers *IEEE Trans. Plasma Sci.* **30** 122–3

[28] Itoh H, Suzuki T, Suzuki S and Rusinov I M 2004 Investigation of ozone loss rate influenced by the surface material of a discharge chamber *Ozone Sci. Eng.* **26** 487–97

[29] Teranishi K, Suzuki S and Itoh H 2004 A novel generation method of dielectric barrier discharge and ozone production using a piezoelectric transformer *Japan. J. Appl. Phys.* **43** 6733

[30] Itoh H, Teranishi K and Suzuki S 2006 Discharge plasmas generated by piezoelectric transformers and their applications *Plasma Sources Sci. Technol.* **15** S51–61

[31] Teranishi K, Shimomura N, Suzuki S and Itoh H 2009 Development of dielectric barrier discharge-type ozone generator constructed with piezoelectric transformers: effect of dielectric electrode materials on ozone generation *Plasma Sources Sci. Technol.* **18** 045011

[32] Teranishi K, Suzuki S and Itoh H 2005 Dielectric barrier discharge generated by piezoelectric transformer in atmospheric pressure *IEEE Trans. Plasma Sci.* **33** 296–7

[33] Norgard P, Kovaleski S, Brayfield R S and Garner A L 2019 High-pressure helium plasma produced in the local electric fields of a piezoelectric transformer *IEEE Trans. Plasma Sci.* **47** 128–35

[34] Teschke M and Engemann J 2009 Piezoelectric low voltage atmospheric pressure plasma sources *Contrib. Plasma Phys.* **49** 614–23

[35] Brockhaus A, Sauerbier R and Engemann J 2009 Comparison of three excitation schemes for cylindrical dielectric barrier discharges *Eur. Phys. J. Appl. Phys.* **47** 22809

[36] Kim H, Brockhaus A and Engemann J 2009 Atmospheric pressure argon plasma jet using a cylindrical piezoelectric transformer *Appl. Phys. Lett.* **95** 211501

[37] Johnson M J, Boris D R, Petrova T B and Walton S G 2019 Characterization of a compact, low-cost atmospheric-pressure plasma jet driven by a piezoelectric transformer *IEEE Trans. Plasma Sci.* **47** 434–44

[38] Babij M, Kowalski Z W, Nitsch K, Silberring J and Gotszalk T 2014 Atmospheric pressure plasma jet with high-voltage power supply based on piezoelectric transformer *Rev. Sci. Instrum.* **85** 054703

[39] Johnson M J and Go D B 2015 Piezoelectric transformers for low-voltage generation of gas discharges and ionic winds in atmospheric air *J. Appl. Phys.* **118** 243304

[40] Lu X, Reuter S, Laroussi M and Liu D 2019 *Nonequilibrium Atmospheric Pressure Plasma Jets: Fundamentals, Diagnostics, and Medical Applications* (Boca Raton: CRC Press, Taylor and Francis Group)

[41] Rosen C A 1956 Ceramic transformer and filters *Proc. Electron Comp. Symp.* 205–11

[42] Warner A W, Onoe M and Coquin G A 1967 Determination of elastic and piezoelectric constants for crystals in class (3 m) *J. Acoust. Soc. Am.* **42** 1223–31

[43] Johnson M J and Go D B 2016 Impingement cooling using the ionic wind generated by a low-voltage piezoelectric transformer *Frontiers Mech. Eng.* **2** 1–11

[44] Jordan N M, Lau Y Y, French D M, Gilgenbach R M and Pengvanich P 2007 Electric field and electron orbits near a triple point *J. Appl. Phys.* **102** 033301

[45] Walsh J L, Iza F, Janson N B, Law V J and Kong M G 2010 Three distinct modes in a cold atmospheric pressure plasma jet *J. Phys. Appl. Phys.* **43** 075201

[46] Ben-Yaakov S and Lineykin S 2006 Frequency tracking to maximum power of piezoelectric transformer HV converters under load variations *IEEE T. Power Electr.* **21** 73–8

[47] Ishii K, Akimoto N, Tashirio S and Igarashi H 1998 Influence of load resistance on higher harmonic voltages generated in a piezoelectric transformer *Japan. J. Appl. Phys.* **37** 5330

[48] Schneider C A, Rasband W S and Eliceiri K W 2012 NIH image to ImageJ: 25 years of image analysis *Nat. Methods* **9** 671–5

[49] Kong M G, Ganguly B N and Hicks R F 2012 Plasma jets and plasma bullets *Plasma Sources Sci. Technol.* **21** 030201

[50] Lu X, Naidis G V, Laroussi M and Ostrikov K 2014 Guided ionization waves: theory and experiments *Phys. Rep.* **540** 123–66

[51] Chang J S, Lawless P A and Yamamoto T 1991 Corona discharge processes *IEEE Trans. Plasma Sci.* **19** 1152–66

[52] Sigmond R S 1984 The residual streamer channel: return strokes and secondary streamers *J. Appl. Phys.* **56** 1355–70

[53] Eilers P H and Boelens H F 2005 Baseline correction with asymmetric least squares smoothing *Leiden Univ. Med. Cent. Rep.* **1** 5

[54] Klarenaar B L M, Guaitella O, Engeln R and Sobota A 2018 How dielectric, metallic and liquid targets influence the evolution of electron properties in a pulsed He jet measured by Thomson and Raman scattering *Plasma Sources Sci. Technol.* **27** 085004

[55] Li Y, Veldhuizen E M, van, Zhang G J, Ebert U and Nijdam S 2018 Positive double-pulse streamers: how pulse-to-pulse delay influences initiation and propagation of subsequent discharges *Plasma Sources Sci. Technol.* **27** 125003

[56] Lu X and Laroussi M 2006 Dynamics of an atmospheric pressure plasma plume generated by submicrosecond voltage pulses *J. Appl. Phys.* **100** 063302
[57] Teranishi K, Suzuki S and Itoh H 2001 Luminous phenomenon of silent discharge using a piezoelectric transformer *Japan. J. Appl. Phys.* **40** 5766
[58] Teranishi K and Itoh H 2005 Absolute measurement of surface potential and discharge power distributions for piezoelectric transformer-based plasma reactor *Japan. J. Appl. Phys.* **44** 7083
[59] Walsh J L, Shi J J and Kong M G 2006 Contrasting characteristics of pulsed and sinusoidal cold atmospheric plasma jets *Appl. Phys. Lett.* **88** 171501
[60] Sretenović G B, Krstić I B, Kovačević V V, Obradović B M and Kuraica M M 2011 Spectroscopic measurement of electric field in atmospheric-pressure plasma jet operating in bullet mode *Appl. Phys. Lett.* **99** 161502
[61] Briels T M P, Kos J, Winands G J J, Veldhuizen E M V and Ebert U 2008 Positive and negative streamers in ambient air: measuring diameter, velocity and dissipated energy *J. Phys. Appl. Phys.* **41** 234004
[62] Luque A, Ratushnaya V and Ebert U 2008 Positive and negative streamers in ambient air: modelling evolution and velocities *J. Phys. Appl. Phys.* **41** 234005